


# Structural Stability and Optical Studies of Poly(3-hexylthiophene) in an ITO/PEDOT:PSS/P3HT Interface

ALINE DOMINGUES BATISTA,<sup>1</sup> WESLEY RENZI,<sup>2</sup>  
JOSE LEONIL DUARTE,<sup>2</sup> and HENRIQUE DE SANTANA <sup>1,3</sup>

1.—Department of Chemistry, CCE, Londrina State University, Londrina, PR 86057-970, Brazil.

2.—Department of Physics, CCE, Londrina State University, Londrina 86057-970, Brazil.

3.—e-mail: hensan@uel.br

An interface between poly(3-hexylthiophene) (P3HT) and poly(3,4-ethylenedioxythiophene) doped with poly(4-styrenesulfonate) (PEDOT:PSS) was prepared in LiClO<sub>4</sub>-acetonitrile (ACN) over indium-doped tin oxide (ITO), known as the ITO/PEDOT:PSS/P3HT system. This system was compared with ITO/P3HT with the aim of studying the stability of aromatic, quinone, and semi-quinone segments in the polymer matrix and also elucidating the influence of the structure on the efficiency of organic photovoltaic cells (OPVs). Initially, Raman spectroscopy was used, varying the laser power to verify the destabilization of radical cation segments to dication segments in the ITO/P3HT system. Electrochemical impedance spectroscopy (EIS) was used to show the behavior of the charged species and the charge-transfer processes of the different P3HT segments as a function of time since preparation of the studied systems. In addition, photoluminescence (PL) and time-resolved PL spectroscopy showed the optical properties of the interfaces formed, based on the different quantities of segments present. It was possible to conclude that the modification introduced into the interface by PEDOT:PSS favors stabilization of the P3HT radical cation segment, which remains stable in this interface for lengthy periods (240 h). This should in turn boost hole extraction, increasing OPV efficiency.

**Key words:** Poly(3-alkylthiophenes), PEDOT/PSS, Raman spectroscopy, electrochemical impedance spectroscopy, organic photovoltaic cells

## INTRODUCTION

Bulk heterojunction organic photovoltaic cells comprise an indium-doped tin oxide (ITO) electrode (anode) interfaced with a photoactive layer. This layer must contain an electron-donor polymer and an electron-acceptor compound, forming multiple interfaces. Poly(3-hexylthiophene) (P3HT) is one of the materials most widely used to form the photoactive layer. It has desirable optical and electrical properties in conjunction with phenyl-C61-butyric acid methyl ester (PCBM), which acts as an electron

carrier.<sup>1–5</sup> To improve hole injection, a thin film of poly(3,4-ethylenedioxythiophene) doped with poly(4-styrenesulfonate) (PEDOT:PSS) can be inserted between the ITO and P3HT. After applying the photoactive layer, a metal electrode (cathode) with high work function<sup>6–10</sup> is inserted.

P3HT can improve the efficiency of such devices and is being thoroughly investigated to identify ways of improving its properties and boost OPV efficiency.<sup>11–14</sup> Spectroscopic techniques are being used as tools for structural investigation of P3HT synthesis conditions, helping to elucidate its stability under the environmental conditions to which it will be subjected.

Moreover, structural characterization of this polymer has also helped us to understand the

electrochemical and charge-transfer processes at work.<sup>12,14</sup> In studies of P3HT and its blends with polydiphenylamine (PDFA) generated over a platinum electrode, electrochemical impedance spectroscopy (EIS) has been used to verify the variations in charge-transfer resistance, and Raman spectroscopy to investigate how these variations are related to shifts in the equilibrium between aromatic, radical cation and dication species in the polymer matrix of this material.<sup>15–17</sup>

In another study on poly(3-methylthiophene) (P3MT), Batista et al.<sup>18</sup> monitored the ITO/P3MT and ITO/PEDOT:PSS/P3MT interfaces as a function of time using *ex situ* Raman spectroscopy after electrochemical synthesis. It was possible to conclude that the radical cation species of the P3MT thiophene ring was more stable in the ITO/PEDOT:PSS/P3MT system. Based on these results, it was inferred that the radical cation form of the PEDOT thiophene ring can be stable at the PEDOT:PSS/P3MT interface and that these segments should also favor stabilization of the P3MT radical cation species, which would make charge injection processes in OPVs a viable proposition.<sup>18</sup>

Similarly, Lima et al.<sup>19</sup> used Raman spectroscopy and EIS to study the ITO/PDFA:P3MT interface as a function of time, comparing it with the ITO/PDFA and ITO/P3MT interfaces to examine the stability of the quinone and semiquinone segments in the blended matrices. It was concluded that, in the ITO/PDFA:P3MT system, the radical cation segments lose stability more slowly than in ITO/P3MT, but both subsequently favor stabilization of the dication segments. The decay of the radical cation segments over time was quantified by electron paramagnetic resonance (EPR) spectroscopy, and the quantity of paramagnetic species per gram of polymer in ITO/P3MT was lower than that found in the blend, indicating that a higher quantity of the cation segment was associated with the ITO/PDFA:P3MT interface.<sup>19</sup>

The aim of this study is to characterize the ITO/PEDOT:PSS/P3HT system using spectroscopic techniques. The Raman spectra of the ITO/P3HT interface obtained by varying the laser power revealed destabilization of the radical cation segments to dication segments in the polymer matrix of the electrochemically synthesized P3HT. EIS was then used to monitor the stabilization of these segments as a function of time since synthesis, based on Bode phase diagrams. Photoluminescence (PL) measurements were taken to verify the optical properties of the different interfaces, and the emission decay time was measured to discuss possible mechanisms for these emissions.

## EXPERIMENTAL PROCEDURES

### Reagents

3-Hexylthiophene (C<sub>10</sub>H<sub>16</sub>S, 99% pure) monomer and 0.8% PEDOT:PSS in H<sub>2</sub>O (conductive inkjet ink) were obtained from Aldrich and used as

received. The support electrolyte was lithium perchlorate (LiClO<sub>4</sub>, 99% pure) supplied by Acros Organics. Acetonitrile (CH<sub>3</sub>CN) [99.5% pure, high-performance liquid chromatography (HPLC) grade] was obtained from JT Baker.

### Electrochemical Synthesis

PEDOT:PSS was previously deposited using the painter method on ITO (sheet resistance 8 Ω/sq to 12 Ω/sq). It was dried at 70°C for 5 min to produce the ITO/PEDOT:PSS system. P3HT was electrochemically synthesized on ITO and ITO/PEDOT:PSS, at potential of +1.80 V applied for 120 s in 0.040 mol L<sup>-1</sup> solution of 3-hexylthiophene monomer in LiClO<sub>4</sub>-acetonitrile (ACN), to produce the ITO/P3HT and ITO/PEDOT:PSS/P3HT systems over an average area of 0.30 cm<sup>2</sup>. For this process, an Autolab PGSTAT 302 N potentiostat/galvanostat was coupled to a microcomputer running NOVA 1.8 software and chronoamperometry (CA) was used. The auxiliary electrode was a platinum plate of area 0.50 cm<sup>2</sup>. Potentials were determined with reference to Ag/AgCl in a Luggin capillary in 0.100 mol L<sup>-1</sup> solution of LiClO<sub>4</sub> in acetonitrile (LiClO<sub>4</sub>-ACN).

### Raman Spectroscopy

Raman spectra were obtained using a DeltaNu Advantage532<sup>®</sup> portable Raman spectrometer, with excitation at 532 nm and set to resolution of 8 cm<sup>-1</sup>. DeltaNu NuSpec software was run using baseline features to remove background fluorescence. Laser power was measured using an Ophir Nova 7Z01500 portable meter.

### Electrochemical Impedance Spectroscopy (EIS)

To obtain open-circuit potential (OCP) impedance diagrams, an Autolab PGSTAT 302 N potentiostat with FRAM32 impedance module was used, varying the frequency from 100 kHz to 0.01 Hz. EIS was performed after preparation and at 24 h, 48 h, 72 h, 96 h, and 240 h. Table I presents the OCP values obtained after the 30 min waiting time and used in EIS measurements.

Although the P3HT films deposited on ITO/PEDOT:PSS were obtained electrochemically at potential of 1.80 V, at which P3HT is electroactive, the OCP values found at the respective EIS measurement times (Table I) were around 0.49 V to 0.85 V, revealing the stability of the studied systems.

### Photoluminescence Spectroscopy and Photoluminescence Decay Time

The films were optically characterized using a 457-nm diode laser for photoluminescence (PL) excitation. The results were recorded using an Ocean Optics USB2000+ spectrometer. Photoluminescence decay times were measured on a FluoTime

**Table I. Open-circuit potentials (OCP) applied during EIS measurements for the systems under study**

System	Time (h)	$E_{OC}$ [V versus Ag(s)/AgCl(s)]
ITO/P3HT	As prepared	0.79
ITO/P3HT	24	0.62
ITO/P3HT	48	0.59
ITO/P3HT	72	0.57
ITO/P3HT	96	0.54
ITO/P3HT	240	0.52
ITO/PEDOT:PSS/P3HT	As prepared	0.85
ITO/PEDOT:PSS/P3HT	24	0.61
ITO/PEDOT:PSS/P3HT	48	0.52
ITO/PEDOT:PSS/P3HT	72	0.52
ITO/PEDOT:PSS/P3HT	96	0.51
ITO/PEDOT:PSS/P3HT	240	0.49

200 (PicoQuant), which uses time-correlated single-photon counting (TCSPC). The equipment incorporates a microchannel plate (MCP) detector, and a 440-nm laser pulsed at 10 MHz was used for detection. The time resolution of the system was 50 ps, with detection range of 300 nm to 800 nm.

## RESULTS AND DISCUSSION

First, any possible structural destabilization of P3HT was monitored. This phenomenon could be induced by the laser power used to obtain the Raman spectra. Raman spectra were obtained as a function of the intensity of the irradiation after preparation of the P3HT film on ITO.

Figure 1 shows the Raman spectra of the ITO/P3HT system as the laser power was varied over the surface of the substrate on which the film was deposited. The laser power settings used were 3.79 mW, 8.60 mW, and 24.04 mW.

The spectra in Fig. 1a and b, obtained at power of 3.79 mW and 8.60 mW, show wider bands in the region between 1400  $\text{cm}^{-1}$  and 1550  $\text{cm}^{-1}$ , characteristic of C=C symmetric and asymmetric stretching of the thiophene ring.<sup>20,21</sup> This widening can be accounted for by the presence of oxidized thiophene ring segments during electrochemical synthesis.<sup>22,23</sup>

The signals at 1445  $\text{cm}^{-1}$  and 1460  $\text{cm}^{-1}$  are respectively related to the quinone and semiquinone segments in the polymer matrix of the P3HT deposited on ITO.<sup>21</sup> The band at 1496  $\text{cm}^{-1}$  was displaced and showed increased intensity, which is characteristic behavior of C=C asymmetric stretching of the thiophene ring. It was originally at 1522  $\text{cm}^{-1}$  and showed low intensity.<sup>20</sup> Previous studies on P3MT and poly(3-octylthiophene) (P3OT)<sup>12,22</sup> have also reported this behavior, and it could indicate that the radical cation segments of the thiophene ring are predominant in the polymer matrix.

However, as seen in Fig. 1c, when the laser power was increased to 24.04 mW, the spectrum was modified compared with the previous spectra.

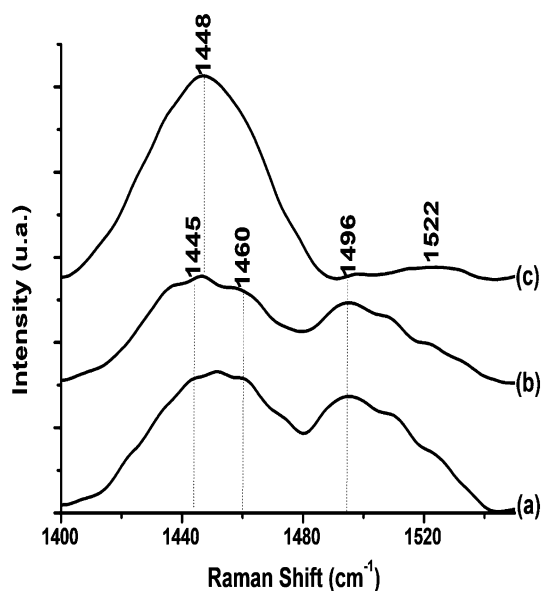


Fig. 1. Raman spectra of ITO/P3HT system with varying laser power: (a) 3.79 mW, (b) 8.60 mW, and (c) 24.04 mW.

This behavior can be understood in terms of the heat induced by the increase in laser power, as observed by Bento et al.<sup>24</sup> in a study on P3OT photodegradation. PL and Raman spectroscopy showed that semiquinone structures changed to quinone structures as a function of laser exposure time.

In view of this limitation on the conditions for obtaining the Raman spectra, it was considered necessary to use another technique to monitor the presence of radical cation segments in the polymer matrix.

With the aim of using EIS to investigate the stability of the radical cation and dication segments in these materials, the results obtained for the ITO/P3HT interface, and subsequently the ITO/PEDOT:PSS/P3HT system, are initially presented and discussed. To do this, Bode phase diagrams were

obtained by determining the phases present in these systems at different time constants.<sup>16,25</sup>

Figure 2 shows the Bode phase diagrams obtained for the ITO/P3HT/LiClO<sub>4</sub>-ACN system at OCP for the interfaces as prepared and after 24, 48, 72, 96, and 240 h had elapsed.

The Bode phase diagrams for the ITO/P3HT/LiClO<sub>4</sub>-ACN system obtained after preparation and up to 72 h later showed two phases, with different phase angle intensities, related to the unipolar (radical cation) and bipolar (dication) charge-transfer processes.<sup>25</sup> The diagrams produced at these times showed that the phase related to unipolar charge transfer occurred with a time constant of 0.011 Hz. Although the unipolar conduction phase was observed at the same time constant for the periods from preparation to 72 h later, note that the intensity of the phase angle decreased as time progressed. The phase of the bipolar charge-transfer process was also observed to shift to higher phase angles over time, with system time constants of 1095 Hz soon after preparation, 398 Hz at 24 h, 321 Hz at 48 h, and 60.2 Hz at 72 h.

After 72 h had elapsed, the results predominantly indicated that the phase related to the bipolar charge-transfer process continued to undergo widening and displacement as a function of time. The resulting Bode phase diagrams in Fig. 2 indicate that the bipolar charge-transfer process related to dication stabilization was favored over time for the ITO/P3HT/LiClO<sub>4</sub>-ACN system.

Figure 3 shows the results of intensities related to the phase angles of the P3HT radical cation and dication segments, obtained from the Bode phase

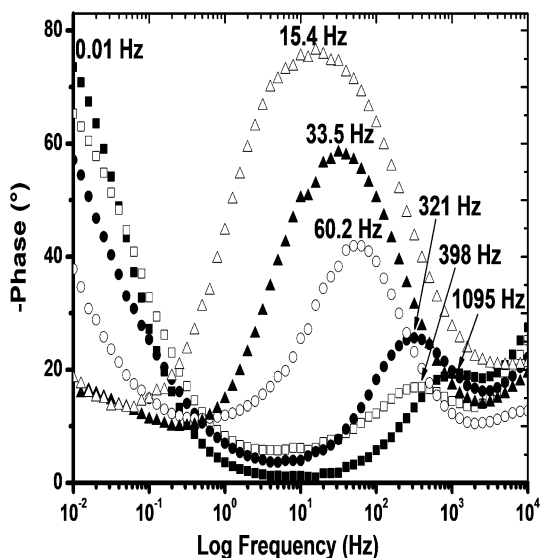


Fig. 2. Bode phase diagrams at open-circuit potential (OCP) for the ITO/P3HT/LiClO<sub>4</sub>-ACN system as a function of time: (■) as prepared, (□) after 24 h, (●) after 48 h, (○) after 72 h, (▲) after 96 h, and (△) after 240 h.

diagrams for the ITO/P3HT/LiClO<sub>4</sub>-ACN system as a function of time.

Figure 3 clearly shows that, as the phase related to the radical cation segment decreased, the phase related to the dication segment increased. Since the radical cation decay observed is accompanied by an increase in the signal related to the dication, symmetrically within the system, the stabilization of the system was thought to be dependent on these segments; i.e., the decay of the phase related to the radical cation segment is a prerequisite for the increase in the phase related to the dication segment.

Figure 4 shows the Bode phase diagrams obtained for the ITO/PEDOT:PSS/P3HT/LiClO<sub>4</sub>-ACN system at OCP for the interfaces as prepared and at 24 h, 48 h, 72 h, 96 h, and 240 h.

The Bode phase diagrams for the ITO/PEDOT:PSS/P3HT/LiClO<sub>4</sub>-ACN system show only one phase at the time constant of 0.01 Hz, related to unipolar charge-transfer processes (radical cation).<sup>25</sup> These results indicate that the P3HT interface with PEDOT:PSS in this system favors stabilization of the P3HT radical cation segment and that it remains stable for the time taken to conduct the experiment (240 h).

This lends weight to the argument in favor of studying interfaces using EIS and Bode phase diagrams. For the ITO/PEDOT:PSS/P3MT system, this method was essential to identify the charge-transfer processes in the different frequency bands and facilitated structural characterization of the interface between P3MT and PEDOT:PSS.<sup>18</sup>

Thus, the EIS results showed that only PEDOT:PSS favors stabilization of the P3HT radical

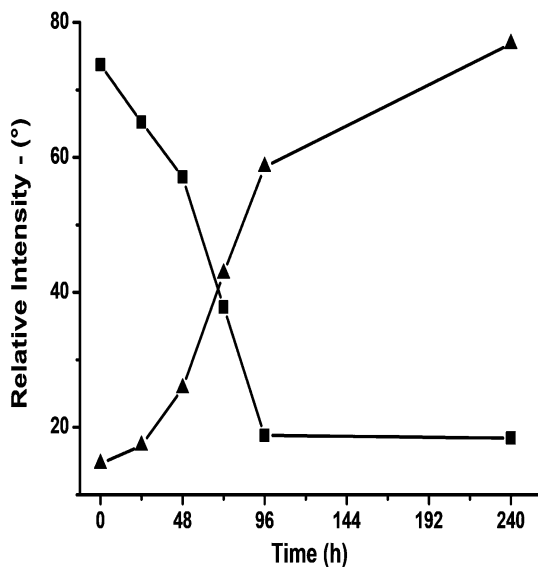


Fig. 3. Phase angle intensities obtained from the Bode phase diagrams for the ITO/P3HT/LiClO<sub>4</sub>-ACN system and related to the P3HT radical cation segments (■) and dication segments (▲) as a function of time (h).

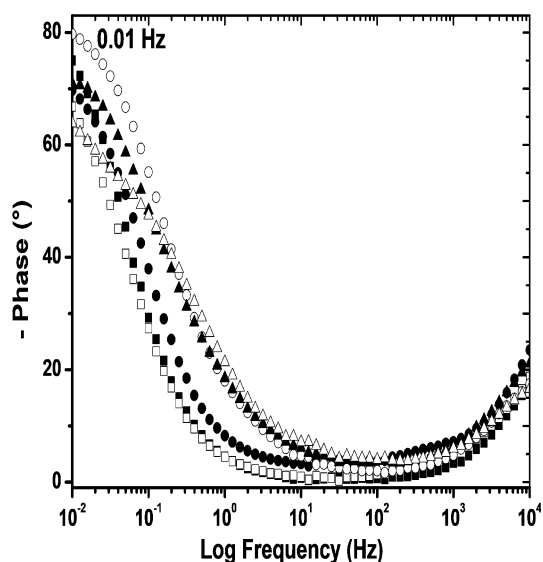


Fig. 4. Bode phase diagrams at open-circuit potential for the ITO/PEDOT:PSS/P3HT/LiClO<sub>4</sub>-ACN system as a function of time: (■) as prepared, (□) after 24 h, (●) after 48 h, (○) after 72 h, (▲) after 96 h, and (△) after 240 h.

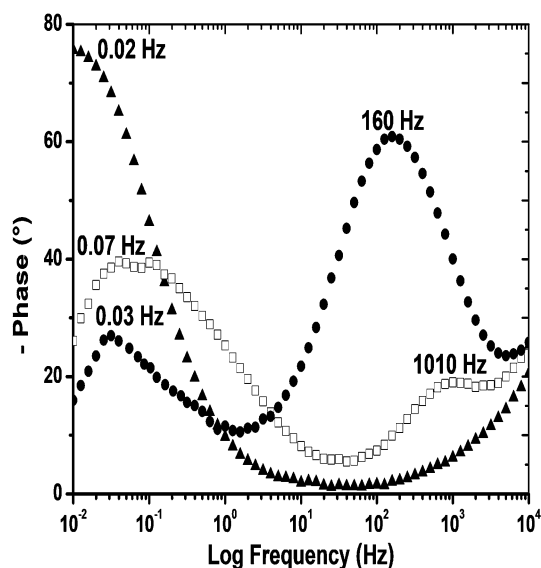


Fig. 5. Bode phase diagrams for the ITO/PEDOT:PSS/P3HT/LiClO<sub>4</sub>-ACN system at applied potentials of: (▲) 1.0 V, (□) 1.2 V, and (●) 1.4 V.

cation segment, and that it remains stable for the time taken to conduct the experiment. Based on this observation, EIS was considered appropriate for obtaining information on the P3HT film deposited over PEDOT:PSS, since the PEDOT:PSS should not influence the information obtained by EIS at the ITO/PEDOT:PSS/P3HT interface. This was observed by studying the ITO/PDFA:P3MT system, with the outermost layer formed by the P3MT.<sup>19</sup> Although deposited on PDFA film, only the P3MT film is considered to participate actively in charge-transfer processes.

On the basis of the EIS results obtained, verifying the high stability of the radical cation segments at the ITO/PEDOT:PSS/P3HT interface, Bode phase diagrams were obtained by applying the potentials at which P3HT oxidation processes occur, as observed by cyclic voltammetry.<sup>15,17</sup> The aim of this experiment is to alter the equilibrium at the interface in order to convert radical cation segments into dication segments.

Figures 5 and 6 show the Bode phase diagrams for the ITO/PEDOT:PSS/P3HT/LiClO<sub>4</sub>-ACN and ITO/PEDOT:PSS/LiClO<sub>4</sub>-ACN systems, respectively, at applied potentials of 1.0 V, 1.2 V, and 1.4 V.

The Bode phase diagrams of the ITO/PEDOT:PSS/P3HT/LiClO<sub>4</sub>-ACN system (Fig. 5) at an applied potential of 1.0 V indicate the presence of only one phase related to the radical cation segment, at a time constant of 0.02 Hz. The observed increase in the time constant could be accounted for by the presence of the PEDOT radical cation (Fig. 6) at this applied potential, since it occurred at a time constant of 0.02 Hz. In a previous study,<sup>18</sup> PEDOT:PSS film showed good electroactivity at the

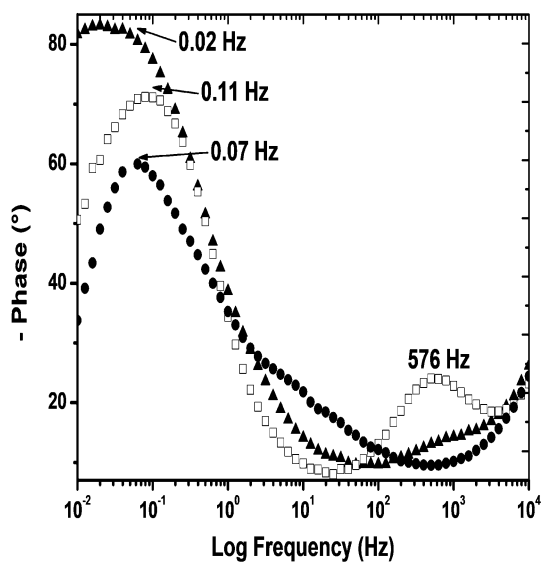


Fig. 6. Bode phase diagrams for the ITO/PEDOT:PSS/LiClO<sub>4</sub>-ACN system at applied potentials of: (▲) 1.0 V, (□) 1.2 V, and (●) 1.4 V.

potential applied to the platinum electrode, using EIS to characterize the radical cation and dication species, in distinct bands of potentials below 0.8 V. However, on the ITO electrode, the displacement of the radical cation toward dication stabilization did not occur; as shown in Fig. 6, at 1.4 V only the drop in the intensity of the phase related to the radical cation was observed in the diagram.

The Bode phase diagrams in Fig. 5, at an applied potential of 1.2 V, show the formation of two phases that are distinct in terms of time constants and displaced frequencies, indicating that the equilibrium displacement process begins when the

potential is applied. At a potential of 1.4 V, there was a decrease in the phase angle related to the radical cation, and an increase in the phase angle and consequent decrease in the frequency related to the bipolar charge-transfer process.

After this study, which verified the presence of the different segments in the P3HT polymer matrix, the optical properties of this material were analyzed by measuring the photoluminescence and luminescence decay time, to better understand the effect of the distribution of the P3HT segments on the emission mechanism of the polymer matrix formed at the ITO/P3HT and ITO/PEDOT:PSS/P3HT interfaces as a function of time.

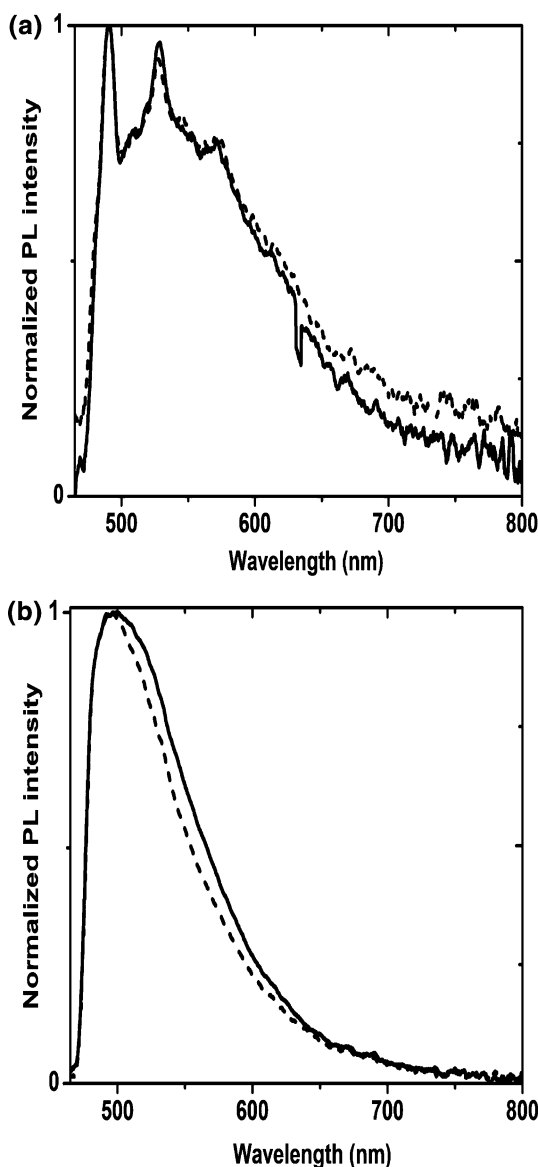


Fig. 7. Photoluminescence spectra for the (---) ITO/P3HT and (—) ITO/PEDOT:PSS/P3HT systems at (a) 0 h and (b) 96 h.

Figure 7 shows the PL spectra obtained from the two interfaces studied at 0 h and 96 h after preparation.

A pattern of behavior was observed in the emission spectra of both materials at 0 h and 96 h. The spectra of the ITO/P3HT and ITO/PEDOT:PSS/P3HT interfaces recorded after preparation (0 h) showed broad and low-intensity emissions, possibly formed by the contributions of three structures in the P3HT matrix: quinone (of higher energy, at around 520 nm), aromatic (at around 570 nm), and semiquinone (of lower energy, ranging from 610 nm to 800 nm).<sup>11</sup> In this case, the emissions from the recently prepared films, with or without PEDOT, show contributions from the three structures with low-intensity emission, as observed in the spectra in Fig. 7a, which show a low signal-to-noise ratio.

The spectra obtained at 96 h (Fig. 7b) show a higher-intensity emission spectrum, with a decrease in intensity in the 610 nm to 800 nm band. Nevertheless, the spectrum of the ITO/PEDOT:PSS/P3HT system showed broader emission between 465 nm and 650 nm, which could indicate that the semiquinone phase is more stable at this interface.

To obtain more information on the optical characterization of the system, the emission decay times of the ITO/P3HT and ITO/PEDOT:PSS/P3HT films were measured at 0 h and 96 h. Decay times are important because they characterize not only the structure and emissions, but also the emission mechanisms. Thus, even where similar spectra are obtained, it is possible in some cases to reveal changes in the decay times and elucidate how they contribute to the mechanism.

The results for the decay times ( $\tau$ ) and how much they contribute (%) are presented in Tables II and III. Table II shows measurements for P3HT deposited directly on ITO, both after preparation and at 96 h.

As observed in the PL spectra, as time progresses, emissions from the films become more intense at higher energies, characterizing emission from different structures. This increase in the quantity of higher-energy chains in the film leads to a decrease in the emission times of the film as a whole, for both more isolated chains ( $\tau_1$ ) and in clusters ( $\tau_2$ ) where energy transfer is facilitated.<sup>26</sup>

According to the results obtained for ITO/P3HT at 0 h and 96 h regarding emissions related to the quinone segment at 527 nm and aromatic segment at 570 nm, the decay times ( $\tau_1$ ) decrease as follows: 527 nm: 1.69 ns to 0.78 ns; 570 nm: 1.28 ns to 0.72 ns. In addition, a change in the decay contributions of  $\tau_1$  was observed (527 nm: from 21% to 43%; 570 nm: from 36% to 52%). The decrease in decay times as well as the increase in the contributions of the faster emissions can be accounted for by the formation of more P3HT quinone and aromatic segments, which would facilitate energy transfer between chains.

**Table II. Emission decay times and decay contributions for ITO/P3HT film measured at 0 h and 96 h**

Detection	0 h		96 h	
	$\tau_1$ (ns) (e, %)	$\tau_2$ (ns) (e, %)	$\tau_1$ (ns) (e, %)	$\tau_2$ (ns) (e, %)
527 nm	$1.69 \pm 0.24$ (21%)	$0.268 \pm 0.009$ (79%)	$0.78 \pm 0.07$ (43%)	$0.169 \pm 0.012$ (57%)
570 nm	$1.28 \pm 0.08$ (36%)	$0.273 \pm 0.008$ (64%)	$0.72 \pm 0.03$ (52%)	$0.199 \pm 0.011$ (48%)

**Table III. Emission decay times and decay contributions for ITO/PEDOT:PSS/P3HT film measured at 0 h and 96 h**

Detection	0 h		96 h	
	$\tau_1$ (ns) (e, %)	$\tau_2$ (ns) (e, %)	$\tau_1$ (ns) (e, %)	$\tau_2$ (ns) (e, %)
527 nm	$1.44 \pm 0.07$ (54%)	$0.211 \pm 0.011$ (46%)	$0.432 \pm 0.084$ (18%)	$0.129 \pm 0.007$ (82%)
570 nm	$1.71 \pm 0.09$ (66%)	$0.190 \pm 0.014$ (34%)	$0.660 \pm 0.130$ (16%)	$0.142 \pm 0.007$ (84%)

Table III presents the decay times and the contributions for P3HT films deposited over the ITO/PEDOT:PSS interface, characterized soon after preparation and at 96 h.

Comparing the results obtained for P3HT with and without PEDOT:PSS, Tables II and III show some highly interesting data related to changes in emission times and contributions.

Based on the results obtained previously by EIS, the use of PEDOT:PSS directly influences the stability of semiquinone segments. This would lead to the conclusion that fewer quinone and aromatic segments would occur at the ITO/PEDOT:PSS/P3HT interface. The increase in the number of semiquinone segments causes an increase in energy/charge transfer between the radical cation segments, directly impacting the drop in decay times (527 nm: from 1.44 ns to 0.432 ns; 570 nm from 1.71 ns to 0.66 ns), and furthermore decreasing the quantity of isolated segments in the film, leading to a drop in the percentage of the longer times (527 nm: 54% to 18%; 570 nm: 66% to 16%).

## CONCLUSIONS

The behavior of P3HT observed in the ITO/P3HT system as a function of different laser powers used to obtain the Raman spectra showed that the laser power intensity caused structural changes in this system, altering the equilibrium between the semiquinone and quinone segments of the thiophene ring in the electrochemically generated material.

It was necessary to use EIS to monitor the structural difference between the ITO/P3HT and ITO/PEDOT:PSS/P3HT systems. The use of PEDOT:PSS considerably favored stabilization of the P3HT radical cation segment, and it remained stable at this interface for a lengthy period (240 h). This effect could account for the

preferential use of this interface for hole extraction and in the increased efficiency of OPVs.

Time-resolved PL measurements were useful for showing that the stability of the species present in the interfaces varied as a function of time after preparation, a crucial parameter affecting the lifetime of the charge-carrying segments of such materials. This type of control could be advantageous for design of devices requiring optical efficiency monitoring.

## ACKNOWLEDGEMENTS

The authors express their appreciation to the Spectroscopy Laboratory (SPEC) at the PROPPG/UEL Multiuser Center. This study was funded by the Araucaria Foundation (09/2016 - PROPPG/UEL 03/2016). A.D.B. would also like to thank the Coordination for the Improvement of Higher Education Personnel (CAPES) for the award granted. The authors also thank the National Council for Scientific and Technological Development for its support.

## REFERENCES

1. S. Antohea, S. Iftimiea, L. Hrosteac, V.A. Antohea, and M. Girtand, *Thin Solid Films* 642, 214 (2017).
2. C.W. Lin, D.Y. Wang, Y.T. Wang, C.C. Chen, Y.J. Yang, and Y.F. Chen, *Sol. Energy Mater. Sol. Cells* 95, 1107 (2011).
3. M.-C. Chen, S. Kar, D.-J. Liaw, W.-H. Chen, Y.-C. Huang, and Y. Tai, *Org. Electron.* 13, 2702 (2012).
4. J. Yang, D. Vak, N. Clark, J. Subbiah, W.W.H. Wong, D.J. Jones, S.E. Watkins, and G. Wilson, *Sol. Energy Mater. Sol. Cells* 109, 47 (2013).
5. D. Momodu, A. Bello, J. Dangbegnon, F. Barzegeer, and N. Manyala, *J. Solid State Electrochem.* 19, 445 (2015).
6. S. Funda, T. Ohki, Q. Liu, J. Hossain, Y. Ishimaru, K. Ueno, and H. Shirai, *J. Appl. Phys.* 120, 33103 (2016).
7. M. Eslamian and J.E. Newton, *Coatings* 4, 85 (2014).
8. T. Stubhan, N. Li, N.A. Luechinger, S.C. Halim, G.J. Matt, and C.J. Brabec, *Adv. Energy Mater.* 2, 1433 (2012).

9. N. Li, T. Stubhan, N.A. Luechinger, S.C. Halim, G.J. Matt, T. Ameri, and C.J. Brabec, *Org. Electron.* 13, 2479 (2012).
10. J. Gilot, M.M. Wienk, and R.A. Janssen, *Adv. Mater.* 22, E67–E71 (2010).
11. D.C. Bento, E.C.R. Maia, T.N.M. Cervantes, R.V. Fernandes, E. Di Mauro, E. Laureto, M.A.T. da Silva, J.L. Duarte, I.F.L. Dias, and H. de Santana, *Synth. Met.* 162, 2433 (2012).
12. H. De Santana, E.C.R. Maia, D.C. Bento, T.N.M. Cervantes, and G.J. Moore, *J. Mater. Sci. Mater. Electron.* 24, 3352 (2013).
13. F.M. Nodari, R.L. Patyk, L.S. Roman, A.R.V. Benvenho, I.A. Hummelgen, E.K.C. Yoshikawa, and J. Gruber, *J. Mater. Sci. Mater. Electron.* 21, 1235 (2010).
14. P. Vanlaeke, A. Swinnen, I. Haeldermans, G. Vanhoyland, T. Aernouts, D. Cheyns, C. Deibel, J. D'haen, P. Heremans, J.S. Poortman, and J.V. Manca, *J. Sol. Energy Mater. Sol. Cells* 90, 2150 (2006).
15. T.N.M. Cervantes, D.C. Bento, E.C.R. Maia, D.A.M. Zaia, E. Laureto, M.A.T. da Silva, G.J. Moore, and H. de Santana, *J. Mater. Sci. Mater. Electron.* 23, 1916 (2012).
16. D.C. Bento, E.C.R. Maia, P.R.P. Rodrigues, G. Louarn, and H. de Santana, *J. Mater. Sci. Mater. Electron.* 24, 4732 (2013).
17. T.N.M. Cervantes, D.C. Bento, E.C.R. Maia, R.V. Fernandes, E. Laureto, G.J. Moore, G. Louarn, and H. De Santana, *J. Mater. Sci. Mater. Electron.* 25, 1703 (2014).
18. A.D. Batista, D.C. Bento, and H. de Santana, *J. Mater. Sci. Mater. Electron.* 28, 1514 (2017).
19. J.H.C. de Lima, D.F. Valezi, A.D. Batista, D.C. Bento, and H. De Santana, *J. Mater. Sci. Mater. Electron.* 29, 6511 (2018).
20. G. Louarn, J.-Y. Mevellec, J.P. Buisson, and S. Lefrant, *Synth. Met.* 55, 587 (1993).
21. M. Baibarac, M. Lapkowski, A. Pron, S. Lefrant, and I. Baltog, *J. Raman Spectrosc.* 29, 825 (1998).
22. E.C.R. Maia, D.C. Bento, E. Laureto, D.A.M. Zaia, E.M. Therézio, G.J. Moore, and H. de Santana, *J. Serb. Chem. Soc.* 78, 507 (2013).
23. D.C. Bento, E.A. Da Silva, C.A. Olivati, G. Louarn, and H. De Santana, *J. Mater. Sci. Mater. Electron.* 26, 7844 (2015).
24. D.C. Bento, E.C.R. Maia, R.V. Fernandes, E. Laureto, G. Louarn, and H. de Santana, *J. Mater. Sci. Mater. Electron.* 25, 185 (2014).
25. G. Lillie, P. Payne, and P. Vagdama, *Sens. Actuators B* 78, 249 (2001).
26. W. Renzi, F. Franchello, N.J.A. Cordeiro, V.B. Pelegati, C.L. César, E. Laureto, and J.L. Duarte, *J. Mater. Sci. Mater. Electron.* 28, 17750 (2017).